**SANDIA REPORT**
SAND2017-10266
Unlimited Release
Printed September 2017

# Experimental and Theoretical Investigation of Shock-Induced Reactions in Energetic Materials

## LDRD Final Report: Project 17-0872

Jeffrey J. Kay, Samuel D. Park, Ian Kohl, Robert Knepper, Darcie Farrow, and Alexander S. Tappan

Prepared by
Sandia National Laboratories
Albuquerque, New Mexico 87185 and Livermore, California 94550

Sandia National Laboratories is a multimission laboratory managed and operated by National Technology and Engineering Solutions of Sandia, LLC, a wholly owned subsidiary of Honeywell International, Inc., for the U.S. Department of Energy's National Nuclear Security Administration under contract DE-NA0003525.

Sandia National Laboratories

Issued by Sandia National Laboratories, operated for the United States Department of Energy by National Technology and Engineering Solutions of Sandia, LLC.



Available to DOE and DOE contractors from
U.S. Department of Energy
Office of Scientific and Technical Information
P.O. Box 62
Oak Ridge, TN 37831

Telephone: (865) 576-8401
Facsimile: (865) 576-5728
E-Mail: reports@osti.gov
Online ordering: http://www.osti.gov/scitech

Available to the public from
U.S. Department of Commerce
National Technical Information Service
5301 Shawnee Rd
Alexandria, VA 22312

Telephone: (800) 553-6847
Facsimile: (703) 605-6900
E-Mail: orders@ntis.gov
Online order: https://classic.ntis.gov/help/order-methods/

SAND2017-10266
Printed September 2017
Unlimited Release

# Experimental and Theoretical Investigation of Shock-Induced Reactions in Energetic Materials LDRD Final Report (Project 17-0872)

Jeffrey J. Kay[1*], Samuel Park[2], Ian Kohl[2], Robert Knepper[2], Darcie Farrow[2], and Alexander S. Tappan[2]
Energetic Materials Reactive and Dynamic Science
[1] *Sandia National Laboratories, P. O. Box 969, Livermore, CA 94551-9053*
[2] *Sandia National Laboratories, P. O. Box 5800, Albuquerque, NM 87185-1454*

## Abstract

In this work, shock-induced reactions in high explosives and their chemical mechanisms were investigated using state-of-the-art experimental and theoretical techniques. Experimentally, ultrafast shock interrogation (USI, an ultrafast interferometry technique) and ultrafast absorption spectroscopy were used to interrogate shock compression and initiation of reaction on the picosecond timescale. The experiments yielded important new data that appear to indicate reaction of high explosives on the timescale of tens of picoseconds in response to shock compression, potentially setting new upper limits on the timescale of reaction. Theoretically, chemical mechanisms of shock-induced reactions were investigated using density functional theory. The calculations generated important insights regarding the ability of several hypothesized mechanisms to account for shock-induced reactions in explosive materials. The results of this work constitute significant advances in our understanding of the fundamental chemical reaction mechanisms that control explosive sensitivity and initiation of detonation.

[*] Principal Investigator. jjkay@sandia.gov

## ACKNOWLEDGMENTS

The authors gratefully acknowledge Michael Armstrong and Joseph Zaug of Lawrence Livermore National Laboratory for assistance implementing ultrafast shock interrogation (USI) and interpreting results. We further acknowledge productive discussions with Yasuyuki Horie (SNL), Sorin Bastea (LLNL), Shawn McGrane (LANL), Katherine Brown (LANL), Betsy Rice (ARL), Brian Barnes (ARL), Craig Tarver (LLNL), and Riad Manaa (LLNL).

## TABLE OF CONTENTS

## FIGURES

# 1. INTRODUCTION: SHOCK-INDUCED REACTIONS IN HIGH EXPLOSIVES

Despite extensive research into the mechanisms by which shock waves initiate chemical reactions in explosives, the reaction processes that take place in response to shock, the physical processes that drive them, and the material properties that promote reaction are not fully understood. Many questions remain unanswered: which chemical bonds break first, what physical processes cause the bonds to break, on what timescale does reaction occur, and how do the molecular structure, crystal structure, and crystalline defects affect the initiation of reaction? The practical results of these shortcomings are that explosive sensitivity is not well understood, initiation of detonation is difficult to model predictively, and the rational design of new materials with desired explosive properties is challenging.

The work described in this report aims to develop a better understanding of the chemical physics of shock-induced reactions in explosive materials, particularly the step-by-step processes by which the mechanical energy of the shock wave triggers initial chemical reactions. Reaction mechanisms are investigated both theoretically and experimentally.

The theoretical work seeks to *evaluate hypothesized chemical reaction mechanisms* as well as *support the ultrafast spectroscopy experiments.* Specific goals of the computational efforts are to:

1. Determine whether strong deformation of molecules, as may occur under shock compression, directly leads to the breakage of chemical bonds. This effect plays a key role in multiple hypothesized reaction mechanisms. The effects of large-amplitude deformation are investigated with *density functional theory (DFT)* calculations on *single molecules.*
2. Determine whether compression of the solid leads to significant closure of the electronic band gap, inducing rapid reactions. This mechanism has been hypothesized previously and is investigated further here. The effect of compression on the electronic band gap is investigated with *density functional theory (DFT)* calculations on *compressed solid crystals*.
3. Support experimental efforts by simulating optical spectra of explosive materials under high degrees of compression. This is accomplished as above with density functional theory calculations on compressed solid crystals.

The experimental work seeks to *understand the dynamics of the initial moments of shock compression,* as well as *identify the conditions that precipitate reaction.* Specific goals of the experimental efforts are to:

1. Characterize the shock conditions (shock velocity, shock stress) required to initiate reaction in shock-compressed explosives. This is accomplished using *ultrafast shock interrogation (USI)*.

2. Observe evidence of reaction, such as spectral signatures of product species. This is accomplished using *ultrafast absorption spectroscopy.*

The results of the above efforts are described in the following sections of this report.

# 2. RESULTS AND DISCUSSION

## 2.1. Theoretical Modeling of Shock-Induced Reactions

### *2.1.1. Single-Molecule Calculations - Response of Molecules to Mechanical Deformation*

Several chemical mechanisms have been developed to explain how shock waves induce reaction in energetic materials [1-7]. At least two of these mechanisms [3-7] involve strong mechanical deformation of molecules prior to the breakage of chemical bonds. The degree of deformation possible in shock-compressed molecular solids (such as high explosives) is expected to be far more severe than would be encountered in chemical reactions at ordinary temperatures and pressures. This places molecules in geometries far from their equilibrium geometry, on portions of their potential energy surfaces that are not normally explored. Work described in this section explores these portions of the potential energy surfaces to determine which types of deformations (stretching, bending, etc.) are effective at breaking chemical bonds.

Density functional theory calculations were performed on three prototypical molecules: nitromethane, 2,4,6-trinitrotoluene (TNT), and 2,4,6-triamino-1,3,5-trinitrobenzene (TATB). Structures of these molecules are shown in Figure 1. Potential energy curves are calculated for several large-amplitude deformations involving the $-NO_2$ functional groups, which are widely expected to be involved in the initial reactions in these types of explosives. Calculations are performed for (*i*) stretching of the R-$NO_2$ bond, (*ii*) bending of the R-$NO_2$ bond, (*iii*) wagging of the $NO_2$ group, and (iv) shear motion of the $NO_2$ group with respect to the remainder of the molecule. Diagrams showing these deformations are shown in Figure 2.

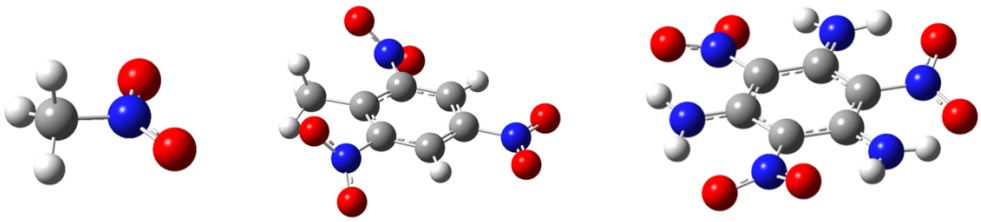

**Figure 1. Molecular structures of nitromethane (left), TNT (center), and TATB (right).**

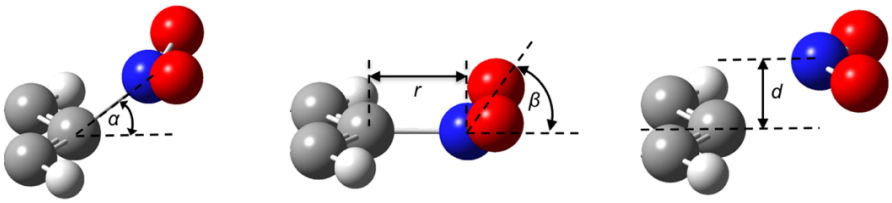


**Figure 2. Molecular deformations considered in this work. $NO_2$ bend (left), $NO_2$ wag and C-$NO_2$ stretch (center), and $NO_2$ shear (right).**

In these calculations, optimized molecular crystal structures are first developed using Møller-Plesset perturbation theory (MP2) with the 6-311++G(2d,2p) basis set. DFT calculations for each type of deformation are then performed using these optimized structures as a starting point. The DFT calculations are performed using the B3LYP hybrid exchange functional with the 6-311++G(2d,2p) basis set, using Gaussian 09 [8]. Calculations are performed on both the ground singlet and ground triplet states, as crossing of the singlet and triplet states is indicative of bond breakage. As Manaa and Fried have shown [9, 10], DFT calculations using the B3LYP functional faithfully reproduce trends observed using more computationally expensive methods.

Representative results are shown in Figure 3. The figure shows the change in energy of the lowest singlet and triplet states of the molecule for four different types of deformations (bend, wag, stretch, and shear). All four motions are effective in breaking the C-$NO_2$ bond in all three molecules, given sufficient displacement, as evidenced by the crossing of the singlet and triplet states.

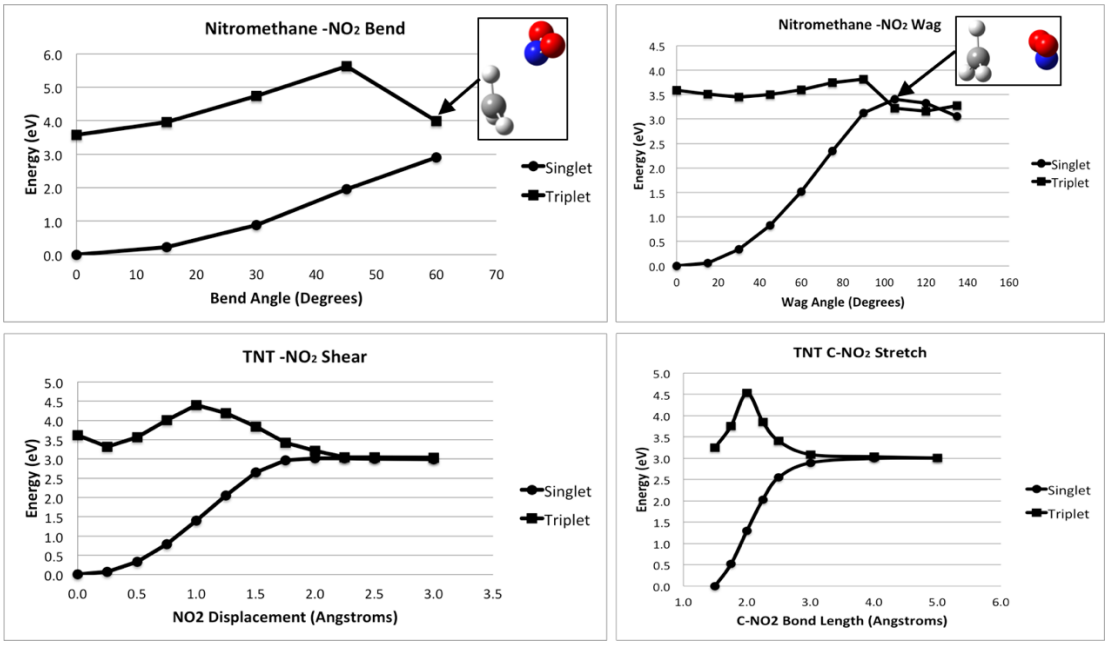


**Figure 3. Change in energy of singlet and triplet states of nitromethane and TNT due to bending motion (upper left), wagging motion (upper right), shearing motion (lower left), and stretching motion (lower right).**

The calculations described here supports previously-developed reaction mechanisms involving bond breakage by high-velocity collisions. Dick *et al*. [6, 7] developed a model known as the "steric hindrance model" for shock-induced reactions to explain the orientation-dependent shock sensitivity of single crystals of PETN. As Dick found in experiments on single crystal PETN, the shock strength required to initiate reaction in PETN depends on the orientation of the incoming shock wave with respect to the principal axes of the crystal [11]. Dick *et al*. explained this in terms of a steric hindrance" model, which states shocks along directions in the crystal with the most steric interactions between neighboring molecules are most likely to lead to reaction. Collisions between neighboring molecules lead to reaction, either by extreme vibrational excitation or by collision-induced fragmentation. These results support collision-induced reaction as a viable mechanism; glancing collisions between adjacent molecules during compressive or shear motion of the lattice can result in bending or shearing of the $NO_2$ groups; given enough collision energy, this can lead to breaking of chemical bonds. Similar phenomena have also been observed in molecular dynamics simulations [12-16].

### *2.1.2. Solid-State Calculations – Change in Electronic Band Gap Under Compression*

One chemical mechanism that has been postulated to explain aspects of shock-induced reaction involves changes in the electronic structure of the solid under compression [4, 5]. By this mechanism, compression of the crystal lattice leads to changes in the electronic structure of the solid; in particular, a decrease in the electronic band gap. A decrease in the electronic band gap decreases the difference in energy between the highest occupied and lowest unoccupied electronic states in the crystal, potentially placing excited states within reach of the ground state and opening a new reaction pathway that is inaccessible in the uncompressed solid. Electronic excitation can potentially occur one of two ways: directly, by complete closure of the band gap, or indirectly, by thermal excitation across a relatively narrow band gap [5].

In this work, the change in band gap of RDX was studied as a function of hydrostatic and uniaxial compression. RDX was chosen for this study because it is among the most extensively characterized secondary explosives, and was also studied experimentally as described in later sections of this report.

Density functional theory calculations were performed using the Vienna Ab-initio Software Package (VASP) [17-20] using generalized gradient methods with the PBE revised for solids (PBEsol) functional [21] and van der Waals corrections [22]. Calculations were performed using hard PAW pseudopotentials [24, 24] and a cutoff of 1250 eV. The hydrostatic compression calculations were performed by first optimizing the known experimental crystal structure of RDX at ambient pressure [25], and iteratively optimizing to a series of increasing hydrostatic pressures. RDX has a phase change ($\alpha$-$\gamma$) at approximately 4 GPa [26-28]; the effects of this phase change were incorporated into the calculations by switching to the $\gamma$ crystal structure [28] for all pressures 4 GPa and above. Uniaxial compression calculations were performed

starting from the optimized structure at ambient pressure, and iteratively contracting the unit cell along one dimension and optimizing the atom positions, up to a compression ratio of $V/V_0 = 0.65$.

Results of the calculations are shown in Figures 4 and 5. Figure 4 shows the band gap of RDX as a function of hydrostatic pressure. The band gap varies from 3.42 eV at 0 GPa to 2.30 eV at 50 GPa ($V/V_0 = 0.6$), and varies smoothly across the $\alpha$-$\gamma$ phase transition at 4 GPa. Figure 5 shows the band gap of RDX as a function of uniaxial compression, along the three principal axes (*a*, *b*, *c*) of the crystal. The uniaxial calculations predict a variation in band gap from 3.42 eV at $V/V_0 = 1$ to 2.28 eV for compression along the *a* axis, 2.61 eV for compression along the *b* axis, and 2.21 eV for compression along the *c* axis at a compression ratio of 0.65.

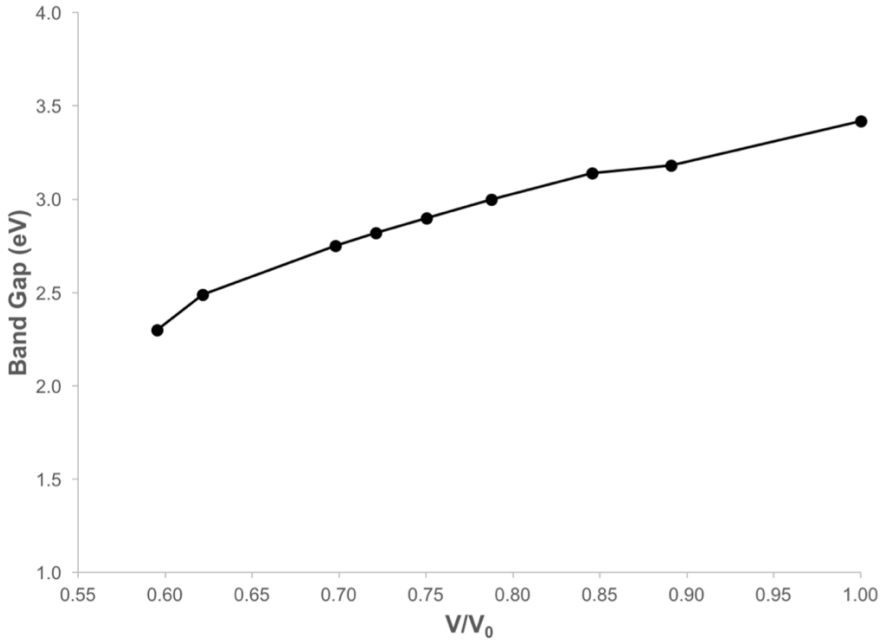


**Figure 4. Calculated electronic band gap of RDX, hydrostatic compression. Pressure varies from 0 GPa at $V/V_0$=1 to 50 GPa at $V/V_0$=0.6.**

Experimental data on the band gap of RDX has been derived from optical absorption spectra [29-32] which indicate an absorption edge at approximately 300 nm, corresponding to a band gap of 4.1 eV. The value of 3.42 eV at ambient pressure compares reasonably well to experimental data and also to previous calculations using GGA methods [33, 34]; generalized gradient calculations tend to under-predict the band gap of solids, to a degree that depends on the material in question. The calculated values here can thus be taken as a lower bound on the band gap of the solid, for any degree of compression, with the true band gap likely to be higher.

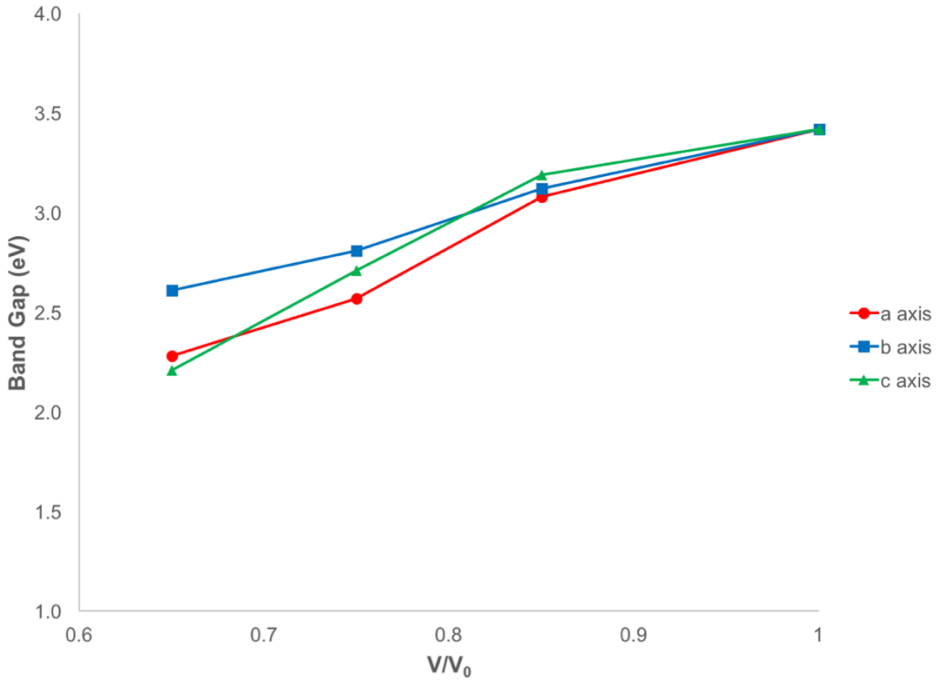


**Figure 5. Calculated electronic band gap of RDX, uniaxial compression.**

Given these lower bounds, the band gap of RDX appears to remain fairly wide even at high states of compression; a band gap of 2.3 eV at 50 GPa, and 2.2 – 2.6 eV under similar degrees of uniaxial stress, indicates that the band gap of the defect-free solid is unlikely to fully close under the conditions thought to exist in detonating materials. The defect-free band gap is also still wide enough to prevent significant thermal excitation across the band gap under compression. It has been shown that crystalline defects may locally lower the band gap of the material [35-37]; effects such as these may still enable reaction under these conditions, but are outside the scope of this study.

### *2.1.3. Solid-State Calculations – Simulated Optical Spectra of Compressed Explosive Crystals*

As part of this study, optical spectra were calculated from the above hydrostatic and uniaxial DFT calculations. Three spectra of uncompressed RDX are shown in Figure 6. The three spectra are calculated as they would appear if a spectrum of the material were taken along each of its three principal axes, and display moderate directional dependence. This directional dependence of the optical spectrum does not appear to have been reported previously. Figures 7 and 8 show, respectively, the calculated optical spectra of RDX under 40 GPa of hydrostatic pressure and RDX uniaxially compressed to $V/V_0 = 0.65$ along its *a* axis. Both spectra show a substantial shift in the absorption edge, 100-150 nm to the red, commensurate with the ~1 eV decrease in band gap under strong compression.

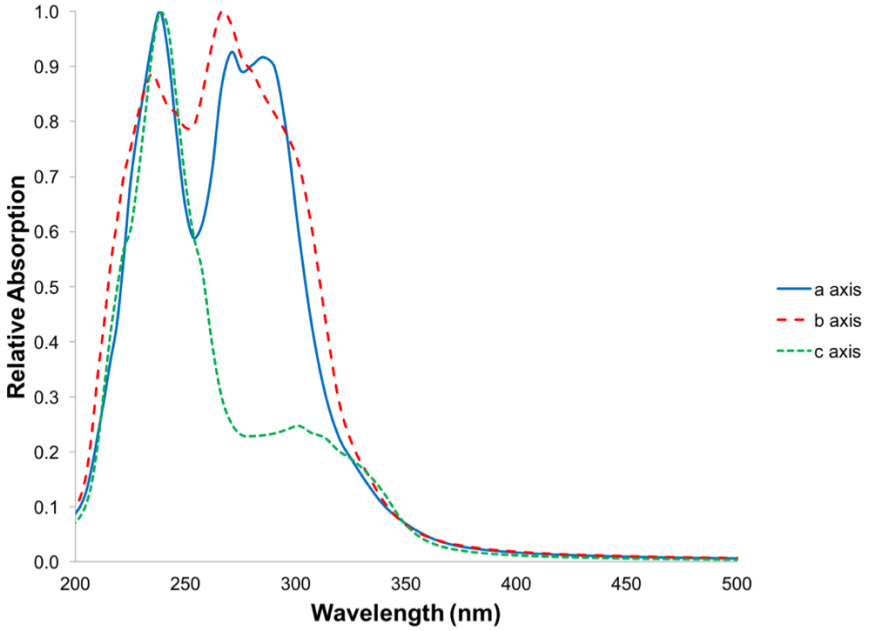


**Figure 6. Calculated optical spectra of uncompressed RDX, as viewed along each of the principal axes of the crystal.**

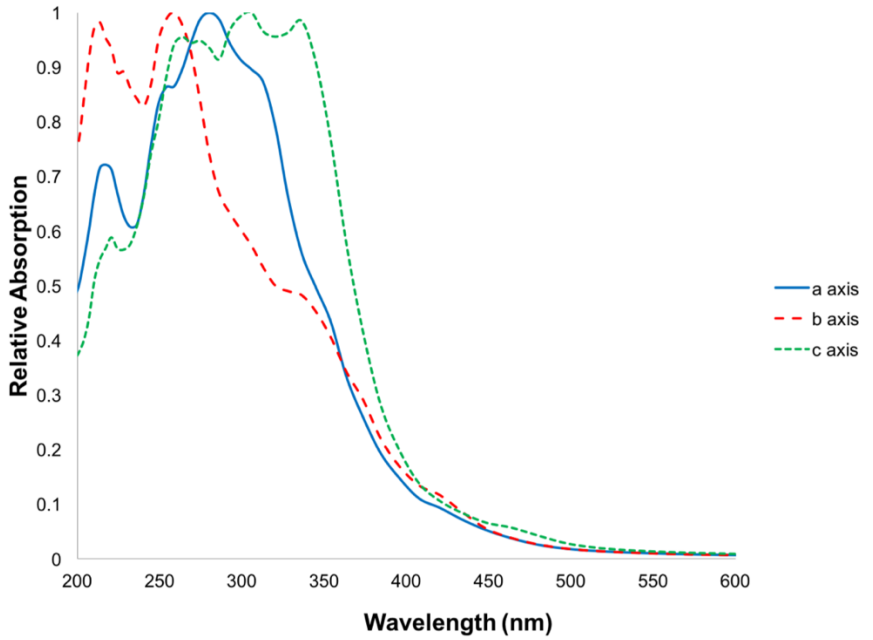


**Figure 7. Calculated optical spectra of RDX under 40 GPa hydrostatic pressure, as viewed along each of the principal axes of the crystal.**

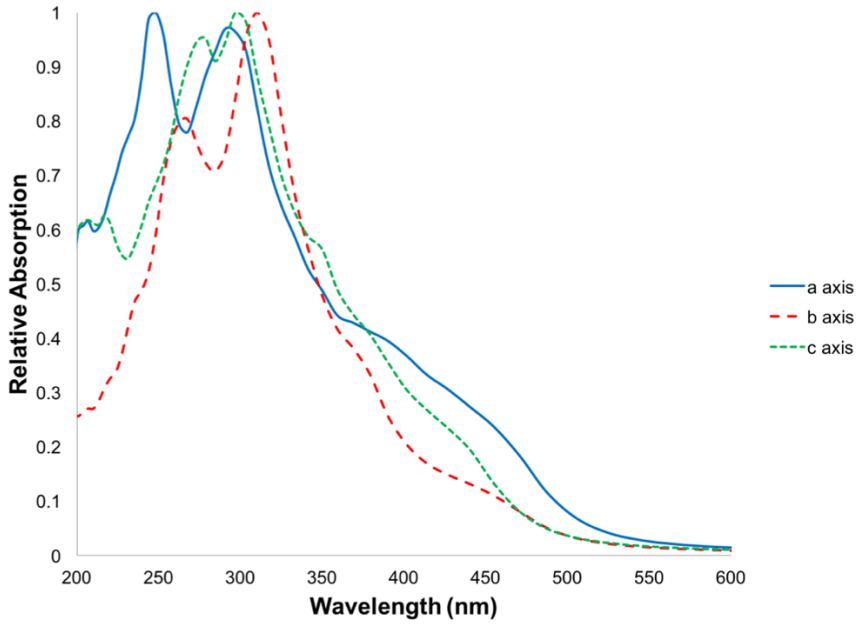


**Figure 8. Calculated optical spectra of RDX uniaxially compressed to $V/V_0$=0.65 along the *a* axis, as viewed along each of the principal axes of the crystal.**

## 2.2. Experimental Investigation of Shock-Induced Reactions

### *2.2.1. Ultrafast Shock Interrogation – Investigating the Timescale Of Reaction*

In the experimental part of this work, laser-driven shock experiments were conducted to investigate shock compression and reaction of explosive materials on ultrafast (picosecond) timescales. Ultrafast shock interrogation (USI) [38] was used to diagnose the shocked state of RDX, PETN, and CL-20 following laser-driven shock compression. USI characterizes the shock velocity and stress attained in shocked samples using interferometry.

In the USI experiments, thin film explosive samples were shocked using ~350 ps, ~800 nm stretched pulses from a regeneratively-amplified Ti:Sapphire laser. The pulses are shaped to produce a steep leading edge with a ~10 ps rise time. The thin film samples consist of a thin glass substrate, with a thin layer of aluminum (~1.5 μm) deposited directly onto the glass, and a thin layer of explosive (~3 μm) vapor-deposed onto the aluminum. The 800 nm laser pulse passes through the glass substrate and ablates the aluminum layer, launching a shock wave into the explosive sample. The USI measurements are performed using a pair of ~350 ps stretched, linearly chirped pulses centered at ~800 nm, which are transmitted through and reflect off of the shocked sample (see Fig. 9). Shock compression of the sample produces a difference in the index of refraction of the compressed material behind the shock front and the

uncompressed material in front of it, resulting in a partial reflection from the traveling shock interface. The partial reflection off of the traveling shock interface interferes with the reflection off of the ablator, encoding the temporal evolution of the shocked sample in a frequency-dependent interference profile that is analyzed with a spectrometer. The shock velocity and stress are determined [38] from the interference profile (see Fig. 10).

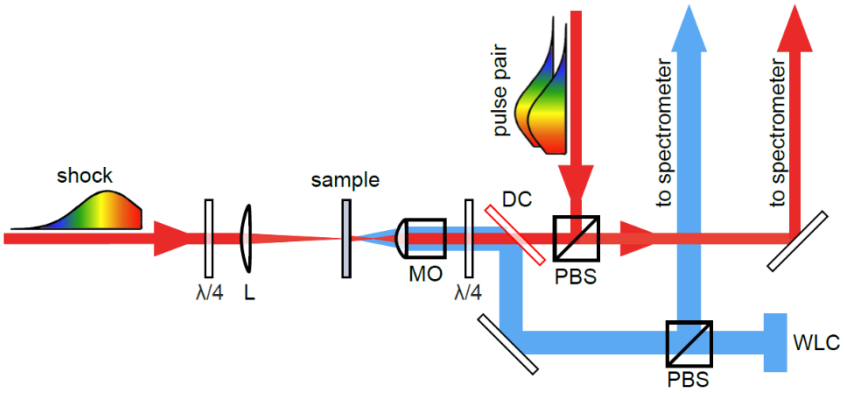


**Figure 9. Diagram of experimental apparatus for laser-driven shock experiments.**

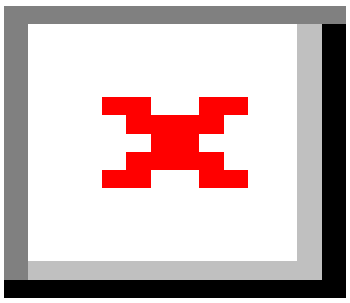

**Figure 10. Example interference signals from USI experiments on PETN.**

USI data on shocked PETN and RDX are shown in Figure 11. The figures show the shock pressure as a function of compression ratio $V/V_0$. The data show a large increase in pressure at $V/V_0 = \sim 0.8$ for both RDX and PETN. At low compression ($V/V_0 > 0.8$) the data lie on the calculated unreacted Hugoniots [39] for both materials; at higher compression, the data lie well above the unreacted Hugoniots.

The low compression ($V/V_0 > 0.8$) data also compare favorably with previous shock Hugoniot measurements published in the literature [40, 41]

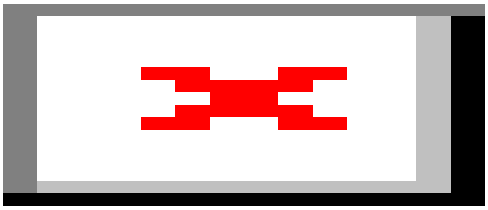

**Figure 11. USI data on shocked PETN (left) and RDX (right). Calculated unreacted and partially-reacted Hugoniots are shown as solid lines.**

The large increases in pressure observed in the data have the characteristics of partial reaction of the materials. Partially-reacted Hugoniots, calculated assuming complete reaction of 10, 20, and 50% of the material with the remainder unreacted, are shown in Figure 10 as solid lines [39]. As can be seen in the figure, the USI data at higher compression lie near these partially-reacted curves. Although it is not expected that a fraction of the material undergoes complete reaction on the timescale of the observations (it is more likely that a *larger* fraction undergoes *partial* reaction), these curves do provide a sense of the effect of exothermic chemistry on the Hugoniot. The measurements thus appear to indicate rapid initiation of exothermic chemistry, on the timescale ~50 picoseconds or less.

### *2.2.2. Ultrafast Absorption Spectroscopy – Support for Shock-Induced Reaction*

To further investigate changes in the electronic structure and/or observation of reaction products, ultrafast absorption spectroscopy experiments were performed on RDX. In these experiments, white-light continuum pulses were used to record the linear absorption spectrum of the material under shock conditions. The experimental arrangement is shown in Figure 9. Continuum pulses are generated by focusing a portion of the compressed ~800 nm beam into a $CaF_2$ crystal, producing broadband radiation with a wavelength range from ~400 to 550 nm. The white light pulses impinge on the sample at normal incidence and are reflected by the aluminum ablator. The reflected white light pulse is then analyzed with a spectrometer.

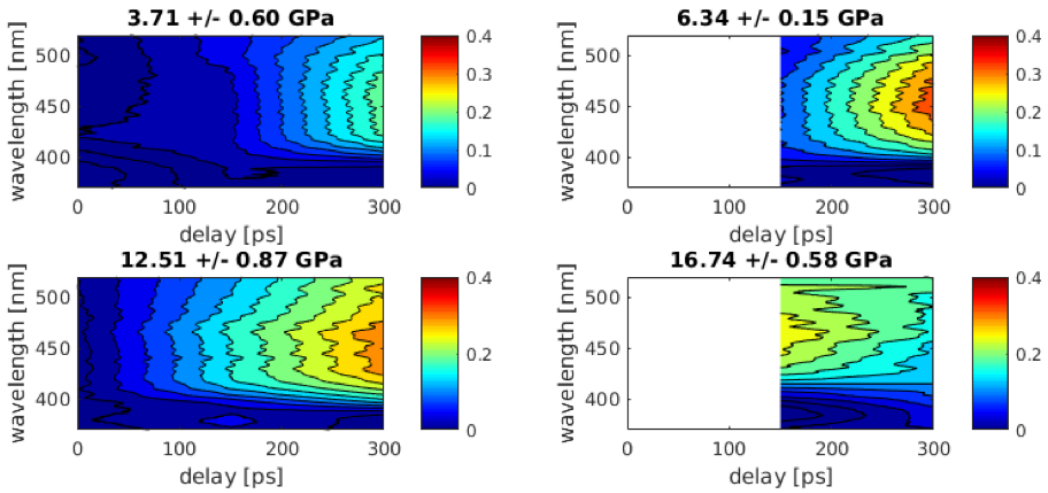


**Figure 12. Ultrafast absorption data on shocked RDX. Blue no absorption; red indicates positive absorption.**

Ultrafast absorption spectra of RDX shocked at pressures of ~3.7 to 16.7 GPa are shown in Figure 12. As the figures show, the sample absorbs light in the wavelength range 400-500 nm after the shock arrives, with a delay that decreases with increasing shock pressure. Uncompressed RDX is transparent at these wavelengths, and compressed RDX should not absorb light across this wavelength range at the pressures attained in the experiment. Absorption due to changes in electronic structure would also occur promptly, rather than increasing with time as observed. The spectra therefore appear to indicate reaction of the material, with the absorption features due to reaction products. $NO_2$, for example, absorbs light across the visible spectrum, and is widely expected to be produced early in the reaction process. While it is not possible to assign the spectral features to a given reaction product at this time, the spectrum does appear to support the occurrence of shock-induced reactions in RDX.

## 3. CONCLUSIONS

Shock-induced reactions in high explosives and their chemical mechanisms were investigated using state-of-the-art experimental and theoretical techniques. Ultrafast shock interrogation and ultrafast absorption spectroscopy were used to interrogate shock compression and initiation of reaction on the picosecond timescale. The experiments appear to indicate reaction of PETN, RDX, and CL-20 on the timescale of tens of picoseconds in response to shock compression, potentially setting new upper limits on the timescale of reaction. Chemical mechanisms of shock-induced reactions were investigated computationally using density functional theory. Single-molecule calculations on large-amplitude deformation indicate that severe bending and shearing motions are able to directly break chemical bonds, supporting previous reaction mechanisms involving high-velocity collisions between molecules. Calculations on

compressed RDX crystals indicate the persistence of a large electronic band gap up to high degrees of compression, and appear to indicate that reaction by reduction of the electronic band gap is unlikely to occur in defect-free RDX. The results of this work constitute significant advances in our understanding of the fundamental chemical reaction mechanisms that control explosive sensitivity and initiation of detonation.

## 4. PRESENTATIONS AND PUBLICATIONS

This work has been presented in the following conference presentations:

1. J. J. Kay, "*Mechanisms of Shock-Induced Reactions in High Explosives",* 2015 American Physical Society Meeting on Shock Compression of Condensed Matter; Tampa, FL, July 2015.
2. J. J. Kay, *"Large-Amplitude Deformation and Bond Breakage in Shock-Induced Reactions of Explosive Molecules",* 2016 American Physical Society March Meeting, Baltimore, MD, March 2016.
3. J. J. Kay, *"Electronic Properties of RDX Under Compression"*, 2017 American Physical Society Conference on Shock Compression of Condensed Matter; St. Louis, MO, July 2017.
4. S. D. Park, M. R. Armstrong, I. Kohl, J. M. Zaug, R. Knepper, A. S. Tappan, S. Bastea, and J. J. Kay, *"Ultrafast Shock Interrogation of Polycrystalline Energetic Materials"*, 2017 American Physical Society Conference on Shock Compression of Condensed Matter; St. Louis, MO, July 2017.

This work has resulted in the following publications:

1. J. J. Kay, *"Mechanisms of Shock-Induced Reactions in High Explosives", AIP Conf. Proc.* **1793***,* 030023 (2017).
2. J. J. Kay, *"Large-Amplitude Deformation and Bond Breakage in Energetic Nitro Molecules"*, to be submitted to *Journal of Chemical Physics*.
3. J. J. Kay, *"Electronic and Optical Properties of RDX Under Compression"*, to be submitted to *Journal of Chemical Physics.*
4. S. D. Park, M. R. Armstrong, I. Kohl, J. M. Zaug, R. Knepper, A. S. Tappan, S. Bastea, and J. J. Kay, *"Ultrafast Shock-Induced Reactions in Pentaerythritol Tetranitrate (PETN) Thin Films"*, to be submitted to *Physical Review Letters.*

## 5. REFERENCES


[1] D. D. Dlott and M. D. Fayer, *J. Chem. Phys.* **92**, 3798 (1990)

[2] A. Tokmakoff, M. D. Fayer, and D. D. Dlott, *J. Phys. Chem.* **97**, 1901 (1993)

[3] J. J. Gilman, *Science* **274**, 65 (1996)

[4] M. M. Kuklja E. V. Stefanovich, and A. B. Kunz, *J. Chem. Phys.* **112**, 3417 (2000)

[5] M. M. Kuklja, *Appl. Phys. A* **76**, 359 (2003)

[6] J. J. Dick, R. N. Mulford, W. J. Spencer, D. R. Pettit, E. Garcia, and D. C. Shaw, *J. Appl. Phys.* **70**, 3572 (1991)

[7] J. J. Dick, *Appl. Phys. Lett.* **60**, 2494 (1992)

[8] *Gaussian 09*, M. J. Frisch, G. W. Trucks, H. B. Schlegel, G. E. Scuseria, M. A. Robb, J. R. Cheeseman, G. Scalmani, V. Barone, B. Mennucci, G. A. Petersson, H. Nakatsuji, M. Caricato, X. Li, H. P. Hratchian, A. F. Izmaylov, J. Bloino, G. Zheng, J. L. Sonnenberg, M. Hada, M. Ehara, K. Toyota, R. Fukuda, J. Hasegawa, M. Ishida, T. Nakajima, Y. Honda, O. Kitao, H. Nakai, T. Vreven, J. A. Montgomery, Jr., J. E. Peralta, F. Ogliaro, M. Bearpark, J. J. Heyd, E. Brothers, K. N. Kudin, V. N. Staroverov, R. Kobayashi, J. Normand, K. Raghavachari, A. Rendell, J. C. Burant, S. S. Iyengar, J. Tomasi, M. Cossi, N. Rega, J. M. Millam, M. Klene, J. E. Knox, J. B. Cross, V. Bakken, C. Adamo, J. Jaramillo, R. Gomperts, R. E. Stratmann, O. Yazyev, A. J. Austin, R. Cammi, C. Pomelli, J. W. Ochterski, R. L. Martin, K. Morokuma, V. G. Zakrzewski, G. A. Voth, P. Salvador, J. J. Dannenberg, S. Dapprich, A. D. Daniels, Ö. Farkas, J. B. Foresman, J. V. Ortiz, J. Cioslowski, and D. J. Fox, Gaussian, Inc., Wallingford CT, 2009.

[9] M. R. Manaa and L. E. Fried, *J. Phys. Chem. A* **102**, 9884 (1998)

[10] M. R. Manaa and L. E. Fried, *J. Phys. Chem. A* **103**, 9349 (1999)

[11] J. J. Dick, *Appl. Phys. Lett.* **44**, 859 (1984)

[12] C. J. Wu F. H. Ree, and C.-S. Yoo, *Propellants Explos. Pyrotech.* **29**, 296 (2004)

[13] A. C. Landerville, I. I. Oleynik, and C. T. White, *J. Phys. Chem. A* **113**, 12094 (2009)

[14] A. Strachan, A. C. T. van Duin, D. Chakraborty, S. Dasgupta, and W. A. Goddard III, *Phys. Rev. Lett.* **91**, 098301 (2003)

[15] S. V. Zybin, W. A. Goddard, P. Xu, A. van Duin, and A. P. Thompson, *Appl. Phys. Lett.* **96**, 081918 (2010)

[16] T.-R. Shan, R. R. Wixom, A. E. Mattson, and A. P. Thompson, *J. Phys. Chem. B* **117**, 928 (2012)

[17] G. Kresse and J. Hafner, *Phys. Rev. B* **47**, 558 (1993)

[18] G. Kresse and J. Hafner, *Phys. Rev. B* **49**, 14251 (1994)

[19] G. Kresse and J. Furthmueller, *Comput. Mat. Sci.* **6**, 15 (1996)

[20] G. Kresse and J. Furthmueller, *Phys. Rev. B* **54**, 11169 (1996)

[21] J. P. Perdew, A. Ruzsinszky, G. I. Csonka, O. A. Vydrov, G. E. Scuseria, L. A. Constantin, X. Zhou, and K. Burke, *Phys. Rev. Lett.* **100**, 136406 (2008)

[22] S. Grimme, J. Antony, S. Ehrlich, and H. Krieg, *J. Chem. Phys.* **132**, 154104 (2010)

[23] P. Bloechl, *Phys. Rev. B* **50**, 17953 (1994)

[24] G. Kresse and D. Joubert, *Phys. Rev. B* **59**, 1758 (1999)

[25] C. S. Choi and E. Prince, *Acta Cryst. B* **28**, 2875 (1972)

[26] B. Olinger, B. Roof, and H. Cady, *Proc. Symposium (Intern.) on High Dyn. Press*., C.E.A. Paris, France 1978, pp. 3-8.

[27] J. A. Ciezak, T. A. Jenkins, Z. Liu, and R. J. Hemley, *J. Phys. Chem. A* **111**, 59 (2007)

[28] A. J. Davidson, I. D. H. Oswald, D. J. Francis, A. R. Lennie, W. G. Marshall, D. I. A. Millar, C. R. Pulham, J. E. Warren, and A. S. Cumming, *Cryst Eng. Comm.* **10**, 141 (2008)

[29] J. Stals, *Trans. Far. Soc.* **67**, 1739 (1971)

[30] P. L. Marinkas, J. E. Mapes, D. S. Downs, P. J. Kemmey, and A. C. Forsyth, *Mol. Cryst. Liq. Cryst.* **35**, 13 (1976)

[31] K. J. Smit, *J. Energet. Mat.* **9**, 81 (1991)

[32] V. Whitley, *AIP Conf. Proc.* **845**, 1357 (2006)

[33] M. W. Conroy, I. I. Oleynik, S. V. Zybin, and C. T. White, *J. Appl. Phys.* **104**, 113501 (2008)

[34] B. L. Ahuja, P. Jain, J. Sahariya, N. L. Heda, and P. Soni, *J. Phys. Chem. A* **117**, 5685 (2013)

[35] M. Kuklja and A. B. Kunz, *J. Phys. Chem. B* **103**, 8427 (1999)

[36] M. Kuklja and A. B. Kunz, *J. Appl. Phys.* **86**, 4428 (1999)

[37] M. Kuklja and A. B. Kunz, *J. Appl. Phys.* **87**, 2215 (2000)

[38] Armstrong, M.R., *et al.*, *J. Appl. Phys.* **108**, 023511 (2010)

[39] S. Bastea, *Personal communication*.

[40] Marsh, S.P., *LASL shock Hugoniot data*. Vol. 5. 1980: Univ of California Press.

[41] Halleck, P. and J. Wackerle, *Dynamic elastic-plastic properties of single-crystal pentaerythritol tetranitrate.* Journal of Applied Physics, 1976. **47**(3): p. 976-982.

## DISTRIBUTION

| | | | |
|---|---|---|---|
| 1 | MS2524 | Basil Hassan | 1510 |
| 1 | MS1454 | Leanna Minier | 2554 |
| 1 | MS1453 | Chris Gresham | 2550 |
| 1 | MS0725 | Jaime Moya | 0600 |
| 1 | MS9053 | Jeffrey Kay | 2554 |
| 1 | MS1454 | Samuel Park | 2554 |
| 1 | MS1454 | Robert Knepper | 2554 |
| 1 | MS1027 | Ian Kohl | 5844 |
| 1 | MS1454 | Alex Tappan | 2554 |
| 1 | MS0836 | Cole Yarrington | 1516 |
| 1 | MS1322 | Aidan Thompson | 1444 |
| 1 | MS1321 | Mitch Wood | 1444 |
| 1 | MS1349 | Hongyou Fan | 1815 |
| 1 | MS9055 | Krupa Ramasesha | 8353 |
| 1 | MS9055 | Craig Taatjes | 8353 |
| 1 | MS9055 | David Chandler | 8300 |
| | | | |
| 1 | MS0899 | Technical Library | 9536 (electronic copy) |
| 1 | MS0359 | D. Chavez, LDRD Office | 1911 |


Sandia National Laboratories